´Zero´-Ripple EMI Input Filter Concepts for Application in a 1-U 500kHz Si/SiC Three-Phase PWM Rectifier

Gerold LAIMER
+41-1-632-7447
laimer@lem.ee.ethz.ch

Johann W. KOLAR
+41-1-632-2834
kolar@lem.ee.ethz.ch

Swiss Federal Institute of Technology (ETH) Zurich
Power Electronic Systems Laboratory
ETH-Zentrum/ETL I16 CH-8092 Zurich
SWITZERLAND / Europe

Abstract. The basic principles of operation and the dimensioning of ´zero´-ripple filter concepts, as known for DC/DC boost converters, is discussed. Based on this a novel ´zero´-ripple input filter for a three-phase PWM rectifier system is proposed. The differential-mode characteristics of the filter and the influence of the filter on the selection of the unity gain bandwidth of the input current control is analyzed by simulations.

1 INTRODUCTION

In [1] a highly compact boost-type three-phase PWM rectifier system (cf. **Fig.1**) has been proposed for the realization of the input stage of a 12kW, wide input voltage range, 2-U telecommunications power supply module. As a next step the rectifier power density should be increased from 5.5kW/dm^3 to 10kW/dm^3 and the construction height should be limited to 1-U. This can be achieved by employing a combination of Si-CoolMOS power transistors and SiC-Schottky-diodes, which facilitates an ultra-high switching frequency of f_p=500kHz, and therefore allows to minimize the volume of the input inductors. However, the input inductors and the EMI input filter required for complying with EMI standards still constitute a considerable share of the overall system volume. Therefore, the application of ´zero´-ripple filter concepts, which have been proposed for DC/DC converters and single-phase PWM rectifier systems [2], is considered. A ´zero´-ripple filter concept allows the partial integration of the input inductors and the EMI filter and provides an attenuation equivalent to a two-stage LC-filter, with the benefit of a lower realization effort.

In this paper, in **Section 2** the input filter attenuation as required by EMI standards is determined. In **Section 3** two ´zero´-ripple filter concepts will be described and compared for an example DC/DC boost converter. Based on this, in **Section 4**, a ´zero-´ripple filter for application in a three-phase PWM rectifier system is proposed. Furthermore, in **Section 5** the passive damping of the filter is described and the influence of the filter characteristic and of the inner mains impedance on the dimensioning of the input current control is discussed in **Section 6**. Finally, in **Section 7** the theoretical considerations are verified by digital simulations.

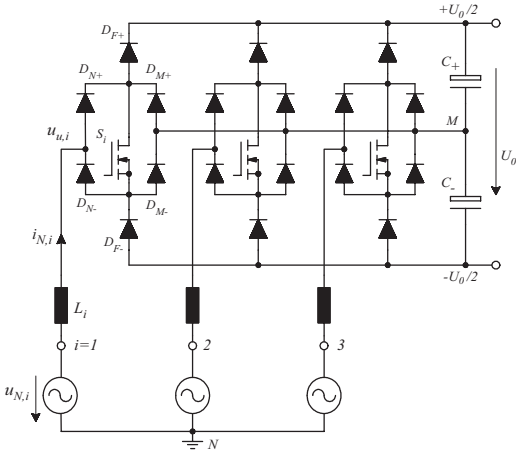

Fig.1: Basic structure of the power circuit of a three-phase/switch/level PWM (VIENNA) Rectifier [1].

2 EMI INPUT FILTER DESIGN CRITERIA

PWM rectifier systems have to comply with the EMI standards EN50081-1/2 (cf. **Tab.1**) and this result in a high switching noise attenuation requirement.

For EMI measurements a line impedance stabilization network (LISN) has to be placed in series with the AC mains (cf. **Fig.2**). Besides defining the inner mains impedance, the LISN (CISPR 16) does provide signal outputs which are connected to the EMI test receiver.

The high frequency common-mode (i_{CM}) and differential-mode (i_{DM}) noise current paths are shown in **Fig.2**(b) for a single phase system. The noise current components, contained in the rectifier input current, are measured as voltage drop across the *50Ω* input resistor of the EMI test receiver (see $u_{LISN,1}$, $u_{LISN,2}$ in Fig.2). There, $u_{LISN,1}+u_{LISN,2}$ corresponds to the common-mode noise current, whereas $u_{LISN,2}-u_{LISN,1}$ is related to the differential-mode noise current.

The rectifier system generates a discontinuous voltage $u_{u,i}$ with switching frequency component, at the input of each bridge leg (cf. **Fig.3)**. There, the fundamental of the mains phase current is formed by the local average value $u_{u,i,avg}$ of $u_{u,i}$ in combination with the sinusoidal mains voltage $u_{N,i}$.

EN 50081-1:1992 (EN 55022 class B)		EN 50081-2:1994 (EN 55011 class A)	
Frequency range	Limits	Frequency range	Limits
0.15-0.5MHz limits decrease linearly with log frequency	66-56dBµV (56-46dBµV)	0.15-0.5MHz	79dBµV (66dBµV)
0.5-5MHz	56dBµV (46dBµV)	0.5-5MHz	73dBµV (60dBµV)
5-30MHz	60dBµV (50dBµV)	5-30MHz	73dBµV (60dBµV)

Tab.1: EMI emissions limits as specified by EN50081-1 (generic emission standard for residential, commercial and light industrial environment) and EN50081-2 (generic emission standard for industrial, scientific and medical (ISM) apparatus) for operation of the test receiver in quasi-peak-detection mode; limits average-peak-detector mode are shown in brackets.

The switching frequency component of $u_{u,i}$ results in a ripple $\Delta i_{L,i}$ of the corresponding phase current (cf. Fig.3) and/or in differential mode noise at the system AC input. Accordingly, an EMI input filter has to be provided which attenuates the amplitudes of the high frequency harmonics of $u_{U,i}$ to the limits as defined by the effective EMI standard.

The simulated spectrum of the rectifier input voltage is depicted in **Fig.4** where the harmonic located at twice the switching frequency, i.e. at $2{\cdot}f_p{=}1MHz$, does show the largest amplitude. Further harmonics with higher amplitudes are present at $f_P{=}0.5MHz$, $3{\cdot}f_p{=}1.5MHz$ and $4{\cdot}f_p{=}2MHz$.

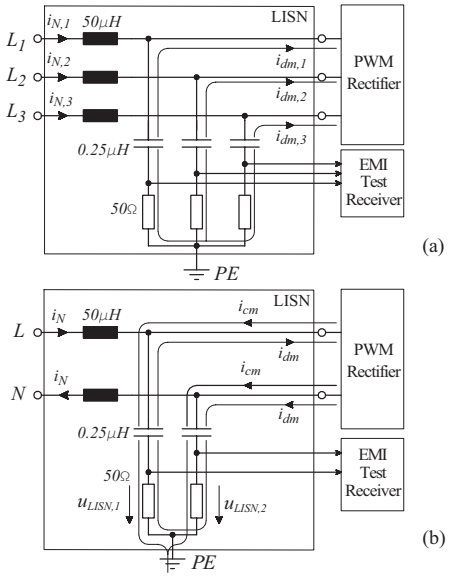

Fig.2: LISN used for coupling the PFC with the ac power supply in a three-phase system **(a)** and in a single-phase system **(b)**. The LISN defines the impedance for PFC looking into the ac power supply and provides a terminal for measuring the conducted noise currents with an EMI test receiver.

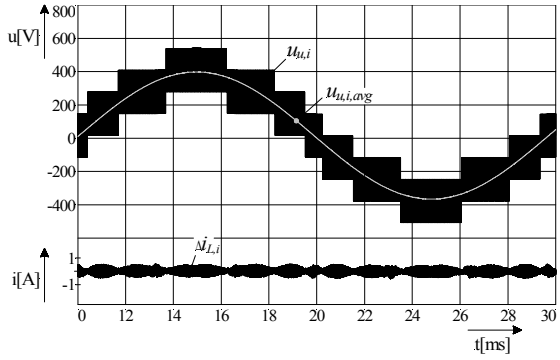

Fig.3: Time behavior of the input voltage $u_{u,i}$ of a rectifier bridge leg with reference to the mains neutral N (see Fig.1) ; $u_{u,i,avg}$ denotes the local average value, and/or the fundamental of $u_{u,i}$ resulting from averaging over a pulse period.

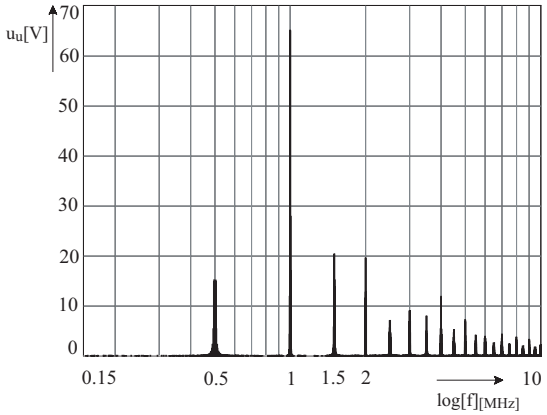

Fig.4: Spectrum of the discontinuous input voltage $u_{u,i}$ of a rectifier bridge leg (cf. Fig.3).

3 ´ZERO´-RIPPLE FILTER CONCEPTS

In this section the basic concepts of ´zero´-ripple filters will be described briefly. For the sake of clarity the considerations are related to a DC/DC boost converter.

3.1 ´Zero´-Ripple Input Filter Concept 1

The conventional realization of a ´zero´-ripple input filter (which is denoted as ZRF_1 in the following) [2], is shown in **Fig.5** for application in a DC/DC boost converter topology. There, we have for the primary and secondary voltages

$$u_p = M\frac{di_1}{dt} + L_p\frac{di_2}{dt}$$
$$u_s = L_s\frac{di_1}{dt} + M\frac{di_2}{dt} \quad . \tag{1}$$

By considering u_1 and u_2, in a first approximation, as ideal constants we have

$$u_1 = u_2 \tag{2}$$

and, therefore, with reference to the circuit topology

$$u_p = u_s \,. \tag{3}$$

Considering Eq.(1) we then can write

$$L_p \frac{di_2}{dt} + M \frac{di_1}{dt} = L_s \frac{di_1}{dt} + M \frac{di_2}{dt} \,. \tag{4}$$

Accordingly, a ´zero´-ripple input current is achieved when

$$\frac{di_2}{dt} = 0 \tag{5}$$

therefore

$$M \frac{di_1}{dt} = L_s \frac{di_1}{dt} \tag{6}$$

and the ´zero´-ripple condition is

$$M = L_s \,. \tag{7}$$

By inserting a transformer equivalent circuit, based on L_p, L_s and M, in Fig.5(a) and considering Eq.(7) it is immediately obvious (cf. Fig.5(b)) that due to the finite capacitance of C_1 and C_2 a finite ripple of the input current i_2 does remain and/or that the ´zero´-ripple filter actually is equivalent to a two-stage LC low-pass filter.

However, a significant advantage of the realization shown in Fig.5(a) as compared to a conventional two-stage filter consists in the fact that only inductor L_p is lying in the main current path. Considering $i=i_1+i_2$ and Eq.(5) we have $di/dt=di_1/dt$, accordingly inductor L_s is carrying only ripple current and can therefore be realized using a wire with small cross-sectional area.

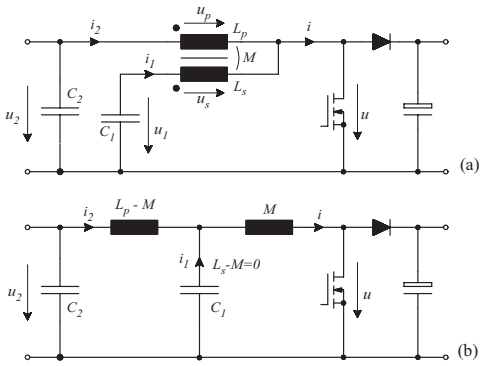

Fig.5: Conventional ´zero´-ripple input filter (ZRF_1, [2]) shown for a DC/DC boost converter **(a)**. Equivalent circuit under consideration of the ´zero´-ripple condition $L_s=M$ **(b)**.

3.2 ´Zero´-Ripple Input Filter Concept 2

The topology of an alternative realization of a ´zero´-ripple filter (in the following denoted as ZRF_2), is depicted in **Fig.6** [3].

There, we have for the transformer primary and secondary voltages

$$\begin{aligned} u_p &= -M \frac{di_1}{dt} + L_p \frac{di}{dt} \\ u_s &= -L_s \frac{di_1}{dt} + M \frac{di}{dt} \end{aligned} \,. \tag{8}$$

where with reference to the circuit topology and for assuming again $u_1=u_2$ (cf. Eq.(2)),

$$u_s = 0 \tag{9}$$

is valid. Considering the node equation $i=i_1+i_2$ and Eq.(8), a ´zero´-ripple input current

$$\frac{di_2}{dt} = 0 \tag{10}$$

results, if

$$\frac{di_1}{dt} = \frac{di}{dt} \tag{11}$$

is valid. With reference to Eq.(9) this can be achieved for

$$0 = -L_s + M \,. \tag{12}$$

Accordingly, the ´zero´-ripple criterion for ZRF_2

$$L_s = M \tag{13}$$

is identical with the ´zero´-ripple criterion for ZRF_1 (cf. Eq.(7)). For replacing the transformer by an equivalent circuit based on L_p, L_s and M, again the equivalence of the basic function of the ´zero´-ripple filter and a two-stage LC low-pass filter can be recognized. As for ZRF_1 (cf. Fig.5) L_p is carrying the load current whereas L_s is carrying only ripple current.

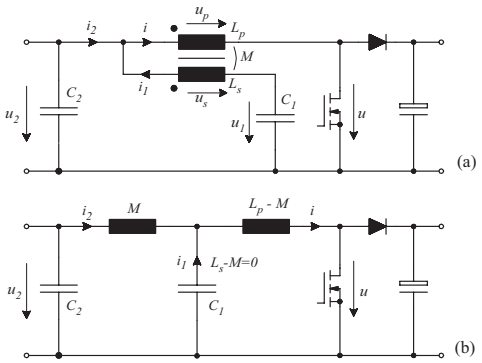

Fig.6: ´Zero´-ripple input filter (ZRF_2) as proposed in [3] shown for a DC/DC boost converter; **(a)** and **(b)** as in Fig.3.

4 PRACTICAL REALIZATION OF A THREE-PHASE ´ZERO´ RIPPLE EMI INPUT FILTER

As explained in Sections 3.1 and 3.2 the ´zero´-ripple filter concepts ZRF_1 and ZRF_2 do offer equal attenuation characteristics. However, as shown in the Appendix, ZRF_2 and ZRF_1 do differ concerning the turns ratio required for realizing the zero ripple condition (see Appendix). ZRF_2 requires fewer turns and since a low number of turns of L_s facilitates the practical realization, ZRF_2 is selected as basis for the following considerations.

The topology of the proposed three-phase ´zero´-ripple filter is depicted in **Fig.7**. The dimensioning of the filter parameters has been carried out, as a first step, using trial-and-error method in combination with a digital simulation of the system behavior.

Starting from an (assumed) maximum admissible input inductor current ripple $\Delta i_{N,i}$ of less than $2A_{pp}$, a minimum input inductance of $L_i=40\mu H$ is required. At high switching speeds a parasitic capacitance of the inductor does significantly increase the power transistor turn-on losses. Accordingly, the inductor has to be realized by connecting multiple inductors in series. Measurements have shown, that the spilt-up of the input inductor into two equal parts, L_p and L_1, provides a sufficiently low parasitic capacitance.

As ZRF_2 requires only a low number of secondary turns (cf. Appendix) a secondary winding L_s is added to only one of the partial input inductor (cf. L_s in Fig.6(b)) resulting in a low manufacturing effort.

Each of the input inductors is realized using two stacked ferrite cores of type EPCOS ELP32-EI (core dimensions: 32x20x10mm^3) with an air gap of $\delta=1.0mm$. The number of turns employed for L_p and L_s is $N_p=8$ and $N_s=2$; this results in $L_p=29\mu H$ and $L_s=2\mu H$ with a mutual inductance of $M=7.2\mu H$. L_1 is realized using $N_1=7$ turns resulting in $L_1=23\mu H$ (all values given are based on measurements).

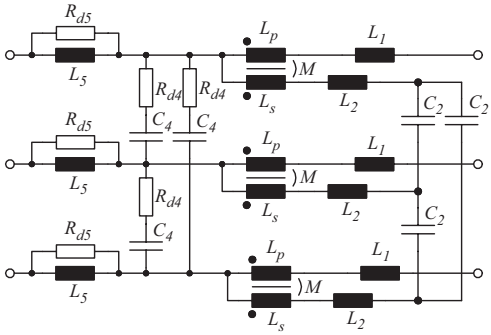

Fig.7: Topology of the proposed three-phase ´zero´-ripple EMI input filter.

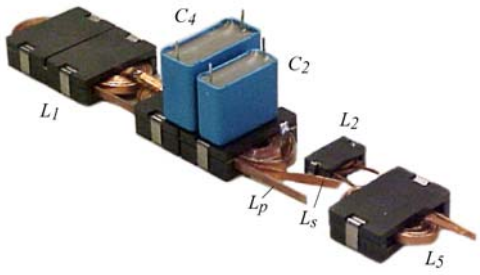

Fig.8: Components of one phase leg of the realized ´zero´-ripple EMI input filter according to Fig.7. The inductor L_5 is carrying only current with mains frequency (no high frequency current ripple is present) and can therefore could be realized using an iron-powder core instead of a ferrite core in order to reduce the filter volume.

For satisfying the ´zero´-ripple condition (cf. Eq.(13)) an additional inductance L_2 with a value of M-$L_s=7.2\mu H$-$2\mu H=5.2\mu H$ has to be connected in series to L_s in order to cancel the inductance in this path. For the sake of clarity, the following considerations will be limited to a single-phase equivalent circuit (cf. **Fig.9**) of the three-phase ´zero´-ripple filter. Therefore, the filter parameters, which are also used for the experimental analysis are:

$L_n = 0...100\mu H$

$L_1 = 23\mu H$	$L_p = 29\mu H$
$L_2 = 5.2\mu H$	$L_s = 2\mu H$
$M = 7.2\mu H$	$L_5 = 8\mu H$
$C_2 = 1\mu F$ (0.33μF)	$C_4 = 2.04\mu F$ (0.68μH)
$R_{d4} = 8\Omega$	$R_{d5} = 0.8\Omega$

(the values for C_2 and C_4 given in parentheses are corresponding to the actual three-phase circuit, cf. Fig.7).

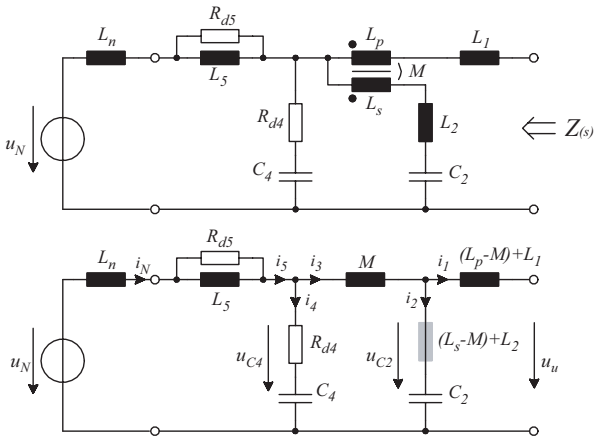

Fig.9: Single-phase equivalent circuit of the three-phase ´zero´-ripple filter shown in Fig.7. The capacitances of C_2 and C_4 do differ from the three-phase system with delta connected capacitors by a factor of three.

5 PASSIVE DAMPING OF THE FILTER

For a real three-phase mains, the inner impedance does vary in a certain range. For the sake of simplicity we assume a purely inductive impedance behavior, $L_n=0...100\mu H$. Due to the wide variation of the inductance an undamped oscillation with the EMI filter input capacitors C_4 and/or C_2 could occur in the case of step-like changes of the mains voltage as e.g. caused by the tripping of a fuse of a faulty system connected in parallel. Active damping of the rectifier EMI input filter is not sufficient in this case, as the rectifier might be connected to the mains but not activated (standby-mode). Therefore, passive damping of the filter has to be provided.

For the damping of the series resonant circuit formed by the inner mains inductance L_n and the filter capacitors C_4, a damping resistor R_{d4} in series with the input capacitor C_4 (cf. Fig.9) is sufficient. The impedance of the filter capacitor C_4 at mains frequency (50/60Hz) is $X_{C4}=1/j\omega C_4=1/(2\pi\cdot 50Hz\cdot 0.68\mu F) = 4.68k\Omega$. Assuming a maximum (line-to-line) input voltage of $U_{N,ll}=480V_{rms}$ the losses occurring in a the damping resistor of $R_{d4}=8\Omega$, which is selected with reference to the characteristic impedance $\sqrt{L_nC_4}$, are only $P=(480V/4.68k\Omega)^2\cdot R_{d4} \sim 85mW$. Therefore, the realization effort as well as the resulting losses and the volume of the component to be employed are negligible.

Unfortunately, damping by R_{d4} is only sufficient for an inner mains inductance of approximately $L_n>20\mu H$. For smaller values of L_n the resonant circuit formed by L_n, C_2 and M is dominating. Sufficient damping of this circuit is more difficult as a damping resistor in series with C_2 is not applicable; C_2 is carrying the switching frequency ripple current which shows an rms-value of several amps, a sufficiently high damping therefore would result in excessive power dissipation. Therefore, a series inductance $L_5=8\mu H$ and a parallel connected damping resistor $R_{d5}=0.8\Omega$ has to be employed. The values for the damping elements L_5 and R_{d5} have been gained by trial-and-error method using digital simulations.

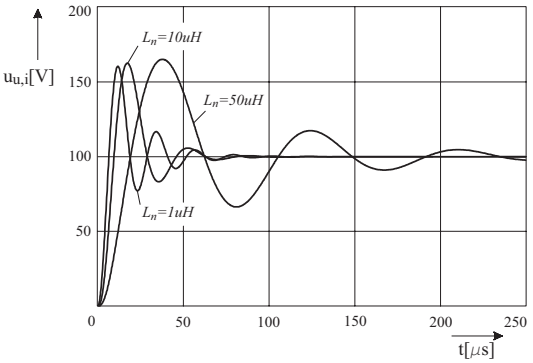

Fig.10: Output voltage $u_{U,i}$ of the input filter (voltage at the rectifier input) resulting for a step change of the mains voltage of 100V and different values for the inner mains inductance L_n.

The step response of the passively damped input filter for different values for the inner mains impedance is shown in **Fig.10**. The resonant overshoot of the filter output voltage (occurring at the rectifier bridge legs) remains below an admissible value of about 70% of the input voltage step. It can also be recognized that the oscillation decays rapidly. A further increase of the damping factor would considerably increase the filter realization effort and also the power losses.

Accordingly, the filter design has to be balanced between low power losses and low realization effort and high damping factor. In practice, independent from passive filter damping an over-voltage protection circuit has to be provided at the rectifier input in order to prevent the system against transient mains voltage spikes.

6 Influence of the EMI Input Filter on the Stability of the Input Current Control Loop

For ensuring stability of the input current control, the EMI input filter has to be included into the contol loop design. One has to determine, in a first step, the overall filter output impedance $Z(s)$ (cf. Fig.9) considering the inner mains inductance L_n. According to **Fig.11** $Z(s)$ essentially shows an inductive behavior.

The design of the current control has to be robust against L_n which could vary over a wide range (cf. section 5). The equivalent circuit shown in Fig.9 leads to the control oriented block diagram for the input current control loop as depicted in **Fig.12**. There, the current information is aquired by an A/D-converter $G_{ADC}(s)$ sampling the current signal eight-times within a switching time period of $T_p=2\mu s$ (oversampling) with a conversion time-delay of $T_{d,ADC}=3/(4T_p)$. An eight-stage moving average filter $G_{mvag}(s)$ is used to suppress the switching frequency components of the sampled current information and this effectively constitutes an average current controller. Both blocks can be modeled as by a delay-time element characterized by $T_d=T_{d,mavg}+T_{d,ADC}=5T_p/4$ using the Pade-approximation

$$G_{pade}(s)=\frac{\frac{1}{12}(\frac{5T_p}{4})^2 s^2-\frac{1}{2}\frac{5T_p}{4}s+1}{\frac{1}{12}(\frac{5T_p}{4})^2 s^2+\frac{1}{2}\frac{5T_p}{4}s+1}. \qquad (14)$$

The PWM power stage $G_{pwm}(s)$ can be approximated by a P-type element as the values of the modulation functions are updated eight-times within a switching period; accordingly, the delay-time of the PWM block is negligible. The resulting open-loop transfer function $F_o(s)=K_iG_{pwm}Z^{-1}G_{pade}$ is depicted in **Fig.13**. For a simple P-type current controller with a gain of $K_i=0.75$ a crossover frequency f_c of *6* to *12kHz* (slope -*20dB/Dec*) results, which is dependent on the inner mains inductance L_n.

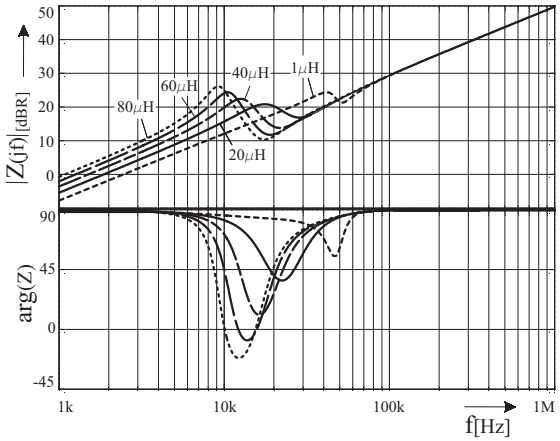

Fig.11: Frequency dependency of the output impedance $Z(jf)$ of the EMI filter (cf. Fig.9).

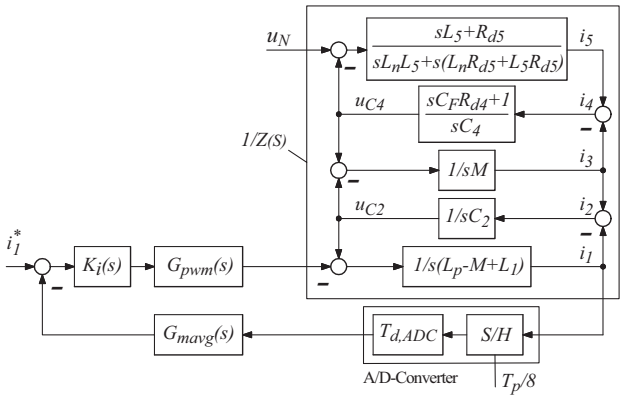

Fig.12: Control-oriented block diagram for the input current control loop.

The phase margin of the open loop transfer function $F_o(s)$ at the crossover frequency is slightly lower than *90°*, accordingly control stability is guaranteed. However, the phase shift is increasing rapidly for higher frequencies due to the delay-time introduced by the A/D conversion and the moving average filter.

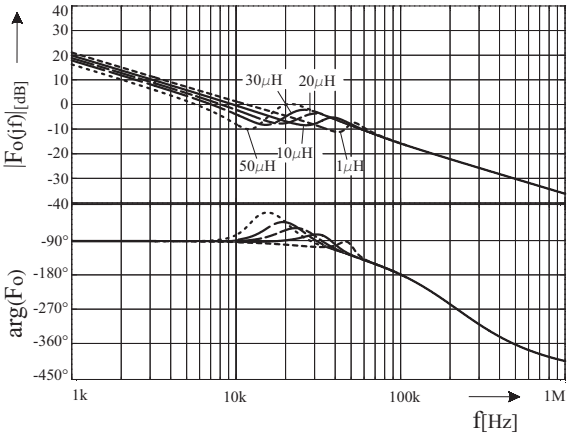

Fig.13: The open loop transfer function of the input current control loop; crossover frequency of *6...12kHz* dependent on the value of the inner mains inductance L_n. The phase margin at the crossover frequency is about 90°, therefore system stability is guaranteed.

As can be seen from the root locus diagram of the open loop system $F_o(s)$ all poles are located in the left half plane (LHP) resulting in a well damped control behavior.

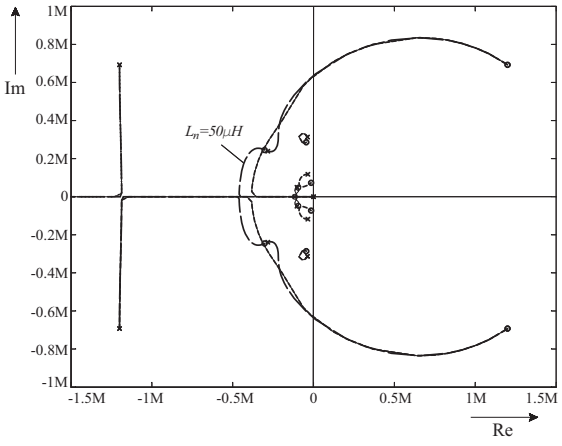

Fig.14: Root locus diagram of the input current control for L_n=*1μH* and L_n=*50μH*. All poles of the closed loop system are located in the LHP. The zeros of the open loop system located in the RHP (and the corresponding poles in the LHP) do result from the Pade-(all-pass)-approximation employed for the modelling of delay-time elements.

7 SIMULATION RESULTS

To verify the performance of the ´zero´-ripple filter, the single-phase equivalent filter is excited with the spectrum of the voltage $u_{U,i}$ generated at the output of a bridge leg of the three-phase PWM rectifier (cf. Fig.4). The resulting noise voltage at the filter input (at the input of the test receiver connected to the LISN, cf. Fig.2) is shown in **Fig.15**.

The noise voltage spectrum shows harmonics with low amplitudes at the switching frequency and at twice the switching frequency. The filter attenuation ensures compliance with the EMI standard EN 50081-2, but is not sufficient for fulfilling the requirements of EN 50081-1 (cf. **Fig.16**). This, however, could be solved by slightly changing the filter parameters (especially by increasing the filter capacitor values) or by adding an additional filter stage.

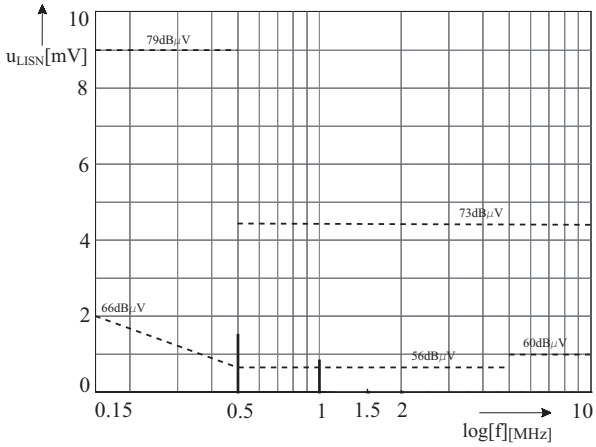

Fig.15: Simulated noise voltage spectrum of the three-phase PWM rectifier system. Limits for the EMI standard EN 50081-1 and EN 50081-2 (cf. Tab.1) are shown by dashed lines.

For determining the sensitivity of the filter characteristic to component tolerances the component values have been varied where the inductors have a tolerance of *±5%* and for the capacitors a tolerance of *±20%*. As one can see immediately from Fig.16, the filter attenuation is not remarkably influenced by parameter variations.

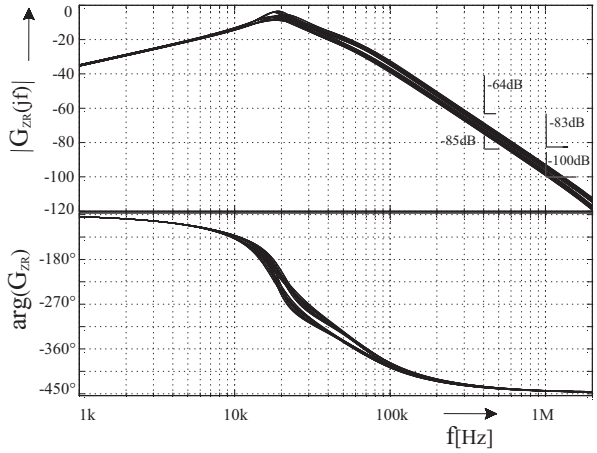

Fig.16: Frequency response of the transfer function of the ´zero´-ripple filter $G_{zr}(s) = u_{LISN} / u_u$. Variations of the filter parameters do no remarkably influence the attenuation characteristic. The given attenuation values are required for complying with EMI standard EN50081-2 (-64dB@400kHz, -83dB@1MHz) and/or with EMI standard EN50081-1 (-85dB@400kHz, -100dB@1MHz) for the noise spectrum of the three-phase PWM rectifier shown in Fig.4.

8 CONCLUSIONS

The three-phase ´zero´-ripple EMI filter concept proposed in this paper allows a partial integration of the EMI input filter and of the input inductor of three-phase PWM rectifier. This results in a low overall realization effort and/or filter volume. The filter characteristic is equivalent to a two-stage LC filter and ensures compliance with the EMI standard EN 50081-2.

In the course of further research the common-mode behavior of the filter will be analyzed by measurements on a 10kW prototype of a 1-U three-phase PWM (VIENNA) rectifier operating at 500kHz switching frequency.

REFERENCES

[1] **Kolar, J. W., and Zach, F.C.:** *A Novel Three-Phase Three Switch Three-Level Unity Power Factor Rectifier.* Proceedings of the 28th International Power Conversion Conference, Nuremberg. Germany, June 28-30, pp. 125-138 (1994).

[2] **Kolar, J. W., Sree, H. Mohan, N. and Zach, F.C.:** *Novel Aspects of an Application of Zero-Ripple Techniques to Basic Converter Topologies.* Proceedings of the 28th IEEE Power Electronics Specialists Conference, St. Louis (MI), USA, June 22-27, Vol.1, pp. 796-803 (1997).

[3] **Schutten, M. J., Steigerwald, R.L., and Sabate, J.A.:** *Ripple Current Cancellation Circuit.* Proceedings of the 18th IEEE Applied Power Electronics Conference, Miami, Feb. 9-13 Vol. 1, pp. 464-470 (2003).

APPENDIX

For inserting a transformer equivalent circuit based on a primary (magnetizing) inductance $L_{\mu P}$, a turns ratio N_P/N_S and a stray inductance $L_{\sigma S}$ referred to the secondary into Figs.5(a) and Fig.6(a) (cf. Fig.A.1(a) and Fig.A.1(b)) we have

$$\begin{aligned} L_P &= L_{\mu P} \\ L_S &= L_{\mu P}\frac{N_S^2}{N_P^2} + L_{\sigma S}\,. \\ M &= L_{\mu P}\frac{N_S}{N_P} \end{aligned} \qquad \text{(A.1)}$$

The ´zero´-ripple condition L_S=M (cf. Eqs.(7) and (13)) then results in

$$L_{\sigma S} = L_{\mu P}\frac{N_S}{N_P}(1-\frac{N_S}{N_P})\,. \qquad \text{(A.2)}$$

For achieving a practically realizable value of the stray inductance, $L_{\sigma S}$>0, we therefore have to select

$$N_S < N_P\,. \qquad \text{(A.3)}$$

The inductance $L_{\mu P}$ can be considered as input inductance of a conventional boost converter where no ´zero´-ripple extension is provided. For employing ZRF_1 and ZRF_2 the inductances

$$\begin{aligned} M &= L_{\mu P}\frac{N_S}{N_P} \\ L_P - M &= L_{\mu P}(1-\frac{N_S}{N_P}) \end{aligned} \qquad \text{(A.4)}$$

are effective. Therefore, an equal attenuation characteristic of ZRF_1 and ZRF_2 is given for (cf. Figs.5(b) and 6(b))

$$(\frac{N_S}{N_P})_{ZRF_1} = (1-(\frac{N_S}{N_P})_{ZRF_2})\,. \qquad \text{(A.5)}$$

In order to limit the ripple of i and/or of i_1 for ZRF_1 to low values a turns ratio Ns/N_P close to *1* is selected. In contrast, only a comparatively low number of turns (cf. Eq.(19)) is required for ZRF_2 to ensure a low ripple of i and i_1. This reduces the realization effort, however, for ZRF_2 L_s and L_p are carrying a current showing a ripple component. For ZRF_1 only i_1 shows a high frequency component. This has to be considered for the dimensioning of the filter concerning core losses and eddy current losses in the windings.

For given turns ratio N_S/N_P now $L_{\sigma S}$ can be calculated based on Eq.(A.2), where under consideration of Eq.(A.5) equal values result for ZRF_1 und ZRF_2. In a practical application $L_{\sigma S}$ is partly realized by an auxiliary inductor connected in series with L_S. Alternatively, the transformer stray inductance could be increased by using a magnetic shunt in between L_1 und L_2.

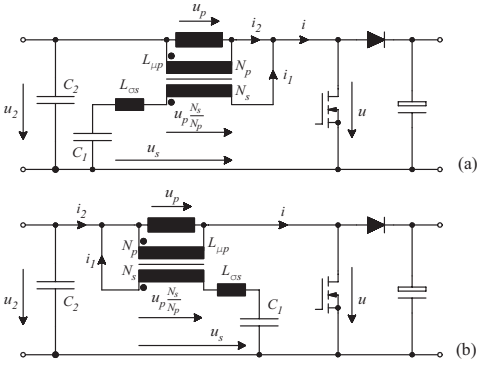

Fig.A.1: Practical realization of ZRF_1 (cf. **(a)**) and ZRF_2 (cf. **(b)**) employing a real transformer ($L_{\mu P}$ denotes the primary (magnetizing) inductance, N_P/N_S is the turns ratio, $L_{\sigma S}$ is the transformer stray inductance referred to the secondary).